Available online at www.sciencedirect.com
SCIENCE DIRECT®
Journal of Solid State Chemistry 178 (2005) 52–57
JOURNAL OF SOLID STATE CHEMISTRY
www.elsevier.com/locate/jssc

Synthesis, structure, and magnetism of Tb_4PdGa_{12} and Tb_4PtGa_{12}

Willa M. Williams[a], M. Moldovan[b], D.P. Young[b], Julia Y. Chan[a,*]

[a]*Department of Chemistry, Louisiana State University, 232 Choppin Hall, Baton Rouge, LA 70803, USA*
[b]*Department of Physics and Astronomy, Louisiana State University, Baton Rouge, LA 70803, USA*

Received 7 July 2004; received in revised form 4 October 2004; accepted 10 October 2004

Abstract

Single crystals of Tb_4MGa_{12} (M = Pd, Pt) have been synthesized. The isostructural compounds crystallize in the cubic space group $Im\bar{3}m$, with $Z = 2$ and lattice parameters: $a = 8.5940(5)$ and $8.5850(3)$ Å for Tb_4PdGa_{12} and Tb_4PtGa_{12}, respectively. The crystal structure consists of corner-sharing MGa_6 octahedra and $TbGa_3$ cuboctahedra. Magnetic measurements suggest that Tb_4PdGa_{12} is an antiferromagnetic metamagnet with a Néel temperature of 16 K, while the Pt analog orders at $T_N = 12$ K.

Keywords: R_4MGa_{12}; Tb_4PdGa_{12}; Tb_4PtGa_{12}; Flux growth; Single-crystal X-ray diffraction; Magnetic susceptibility; Cuboctahedra; Metamagnet; Gallides; Rare earth intermetallics

1. Introduction

The ternary compounds Ce_nMX_{3n+2} ($n = 1$, 2; ∞; M = Co, Rh, Ir; X = Ga, In) [1–5] have received a great deal of attention within the last few years. This system possesses a very rich magnetic phase diagram that allows one to probe ground states with long-range magnetic order, superconductivity, and quantum criticality. $CeMIn_5$ (M = Co, Rh, Ir) forms tetragonal structure composed of alternating layers of $CeIn_3$ cuboctahedra and "MIn2" rectangular prisms [6,7]. The quasi-two-dimensional layered structure is highly anisotropic. $CeMIn_5$ (M = Co, Ir) exhibit heavy fermion superconductivity under ambient conditions at $T_c = 2.3$ and 0.4 K, respectively [7]. $CeRhIn_5$ superconducts at 2.1 K under applied pressures of 16 kbar [3]. $CeRhIn_5$, under ambient pressure, is a heavy-fermion antiferromagnet with $T_N = 3.8$ K [1,8]. Similarly, Ce_2MIn_8 ($n = 2$; M = Rh, Ir) consists of one layer of MIn2 rectangular prisms alternating with two layers of $CeIn_3$ cuboctahedra [9]. Ce_2RhIn_8 orders antiferromagnetically at $T_N = 2.8$ K at ambient pressure and superconducts at 2.1 K under a pressure of 25 kbar [9]. $CeIn_3$ ($n = \infty$) is antiferromagnetic ($T_N = 10$ K) and superconducts ($T_c = 0.25$ K) under a pressure of 25 kbar [10].

In our search for Pd and Pt containing intermetallics, we have discovered several Ce–Pd–Ga phases. $CePdGa_6$ is a heavy fermion metamagnet ($\gamma \sim 230$–360 mJ/mol K^2), in which the Ce f-moments order antiferromagnetically along the c-axis at $T_N = 5.5$ K. A reconfiguration of spins induces a ferromagnetic moment in the ab-plane [11]. Ce_2PdGa_{12} orders antiferromagnetically at $T_N \sim 11$ K with a spin reconfiguration transition at 5 K and has recently been compared to Ce_2PdGa_{10} which exhibits large positive magnetoresistance of over 200% at 9 T [12].

Other Ce–Pd–Ga phases have also been reported. $Ce_8Pd_{24}Ga$ orders antiferromagnetically at $T_N = 3.6$ K and exhibits an enhanced electronic specific heat at $T = 10$ K [13]. CePdGa exhibits an antiferromagnetic transition at $T_N = 1.8$ K [14]. $CePd_2Ga_3$ orders ferromagnetically at $T_c = 6$ K [15,16]. $CePd_2Ga$ (YPd_2Si-type) order antiferromagnetically at a Néel temperatures of [13,17]. Rare earth intermetallics containing Sm or Tb were also investigated because of the possibility of mixed

*Corresponding author. Fax: +1 225 578 3458.
E-mail address: jchan@lsu.edu (J.Y. Chan).

0022-4596/$ - see front matter © 2004 Elsevier Inc. All rights reserved.
doi:10.1016/j.jssc.2004.10.026

valency or other unusual magnetic or electronic behavior. $SmPd_2Ga_2$, of the $ThCr_2Si_2$ structure type, has been discovered to exhibit large positive magnetoresistance which increases by almost 100% at low temperature [18].

Magnetic ordering is also found in terbium intermetallics. A study by neutron diffraction shows that orthorhombic TbNiGa orders antiferromagnetically at $T_N = 23$ K [19]. $TbNi_3Ga_2$ (YCo_3Ga_2-type) orders ferromagnetically below 14 K [20]. Tb_2CoGa_3 orders ferromagnetically below 28 K [21]. TbPdGa exhibits a complicated magnetic structure which undergoes a magnetic transformation at 26 K [22]. TbPtGa and TbRhGa of the orthorhombic TiNiSi-structure type are antiferromagnetic with Néel temperatures of 34 and 22 K, respectively [22,23]. Finally, $TbGa_2$ exhibits a multi-step metamagnetic transition at $T_N = 18$ K when the field is applied perpendicular to the *c*-axis [24], while $TbGa_6$ ($PuGa_6$-type), exhibits pressure-induced superconductivity ($T_c = 6$ K) at ~10 kbar [25].

Neutron and single crystal X-ray studies of $RE_4FeGa_{12-x}Ge_x$ (RE = Sm, Tb) reveal that these compounds crystallize in the cubic $U_4Re_7Si_6$-type ($Im\bar{3}m$) with lattice parameters $a = 8.657(4)$ Å and 8.5620(9) Å for Sm and Tb analogs, respectively [26]. $Tb_4FeGa_{12-x}Ge_x$ orders antiferromagnetically at a Néel temperature of 13 K, while the isostructural Sm analog does not exhibit any magnetic ordering [26].

The crystal structure and transport measurements on polycrystalline R_4MGa_{12} (R = Gd–Lu; M = Ni, Pd) were reported [27]. The structure of R_4MGa_{12} (R = Gd–Lu; M = Ni, Pd) is cubic and can be viewed as a redistributed homolog of $U_4Re_7Si_6$-type [28] or alternatively, the structure can be regarded as the result of partially filling the octahedral voids in the cubic close packed $AuCu_3$-type [29]. The electrical resistivity of R_4MGa_{12} (R = Gd–Lu; M = Ni, Pd) shows metallic behavior [27]. In this paper, we report the crystal structure, transport and magnetic properties of single crystals of Tb_4PdGa_{12} and Tb_4PtGa_{12}.

2. Experimental

2.1. Syntheses

The samples were synthesized from small pieces of Tb metal (99.9%, Alfa Aesar), Pd and Pt powder (99.998%, Alfa Aesar), and Ga pieces (99.99999%, Alfa Aesar). Single crystals were grown by placing constituent elements in an aluminum oxide crucible in a molar ratio of 1:1:20. The sample was sealed in an evacuated fused silica tube and heated to a temperature of 1150 °C for 7 h and then cooled at a rate of 15°C/h to 530 °C, at which point the excess Ga flux was removed by centrifugation. The synthesis yielded cuboidal-shaped crystals which ranged in size from 0.02 to 0.5 mm^3.

2.2. Single crystal X-ray diffraction

A single crystal fragment of ~0.02 mm × 0.04 mm × 0.06 mm (Tb_4PdGa_{12}) and ~0.02 mm × 0.04 mm × 0.08 mm (Tb_4PtGa_{12}) were mechanically extracted, placed on a glass fiber and mounted on the goniometer of a Nonius Kappa CCD diffractometer equipped with Mo$K\alpha$ radiation ($\lambda = 0.71073$ Å). Additional data collection and crystallographic parameters are presented in Table 1. To ensure sample homogeneity several single crystals from several different sample growths were characterized by single crystal X-ray diffraction. Crushed single crystals were also characterized by powder X-ray diffraction to confirm sample homogeneity.

The structures were solved using direct methods (SHELXL97) [30]. Data were then corrected for extinction and refined with anisotropic displacement parameters. Atomic coordinates and related structural information is provided in Table 2. Selected interatomic distances and bond angles are given in Table 3. The stoichiometries of the samples were determined by dividing the site multiplicity of each atomic position by the multiplicity of the atomic position with the

Table 1
Crystallographic parameters

Crystal data		
Formula	Tb_4PdGa_{12}	Tb_4PtGa_{12}
a (Å)	8.5940(5)	8.5850(3)
V (Å^3)	634.73(6)	632.73(4)
Z	2	2
Crystal dimension (mm^3)	0.02 × 0.04 × 0.06	0.02 × 0.04 × 0.08
Crystal system	Cubic	Cubic
Space group	$Im\bar{3}m$	$Im\bar{3}m$
θ range(deg.)	3.5–30.0	3.36–30.0
μ (mm^{-1})	48.260	58.034
Data collection		
Measured reflections	718	715
Independent reflections	117	118
Reflections with $I > 2\sigma(I)$	109	100
R_{int}	0.1060	0.0914
h	−12→12	−12→12
k	−8→8	−8→8
l	−8→8	−8→8
Refinement		
[a] R [$F^2 > 2\sigma(F^2)$]	0.0454	0.0257
[b] $wR(F^2)$	0.1189	0.0512
Reflections	109	116
Parameters	10	10
$\Delta\rho_{max}$ (e Å^{-3})	2.809	2.077
$\Delta\rho_{min}$ (e Å^{-3})	−3.319	−2.010
Extinction coefficient	0.00433(8)	0.00378(6)

[a] $R = \sum||F_o| - |F_c||/\sum|F_o|$.
[b] $wR = \sum[w(F_o^2 - F_c^2)]/\sum[w(F_o^2)^2]^{1/2}$.

Table 2
Atomic positions and thermal parameters of Tb_4MGa_{12} (M = Pd, Pt)

		x	y	Z	U_{eq}[a] (Å^2)
Tb1	8*c*	3/4	3/4	3/4	0.0082(1)
Pd1	2*a*	0	0	0	0.0057(7)
Ga1	12*d*	1/2	0.204366(3)	3/4	0.0073(8)
Ga2	12*e*	1/3	0	0	0.0060(1)
Tb1	8*c*	3/4	3/4	3/4	0.0084(3)
Pt1	2*a*	0	0	0	0.0072 (3)
Ga1	12d	1/2	0.203989(2)	3/4	0.0089(4)
Ga2	12*e*	1/3	0	0	0.0070(4)

[a] U_{eq} is defined as one-third of the trace of the orthogonalized $\mathbf{U}_{ij}$ tensor.

Table 3
Selected inter-atomic distances and bond angles of Tb_4MGa_{12} (M = Pd, Pt)

	Interatomic distances (Å)	
	Tb_4PdGa_{12}	Tb_4PtGa_{12}
Cuboctahedra		
Tb1–Ga1 (× 6)	3.03844(18)	3.0526(11)
Tb1–Ga2 (× 6)	3.0641(4)	3.05994(11)
Ga1–Ga2	2.7730(19)	2.7746(2)
	Angles (°)	
Cuboctahedra		
Ga1–Tb–Ga2 (× 4)	54.05(4)	54.20(4)
Ga1–Tb–Ga2 (× 4)	90.0	90.0
Ga1–Tb–Ga2 (× 4)	125.959(4)	125.80(6)
Octahedra		
M–Ga2 (× 6)	2.544(3)	2.5341(3)

smallest coefficient. Elemental analysis was performed using a Hitachi S-3600N Variable Pressure Scanning Electron Microscope (VP-SEM) with integrated energy dispersive spectroscopy (EDS) capabilities.

2.3. Property measurements

Transport and magnetic measurements were performed on single crystals of Tb_4MGa_{12}.The electrical resistance was measured by the standard 4-probe AC technique at 27 Hz with a current of 1 mA. 1-mil Pt wires were attached to the sample with silver epoxy. The magnetic susceptibility measurements were made using a commercial magnetometer (Quantum Design). The samples were zero-field-cooled (ZFC) to 2 K and then warmed to room temperature in a constant DC field of 1000 G.

3. Results and discussion

3.1. Structure

The structures of Tb_4MGa_{12} (M = Pd, Pt) are provided in Fig. 1. Tb_4MGa_{12}, (M = Pd, Pt) of the Y_4PdGa_{12}-structure type [27] crystallize in the cubic $Im\bar{3}m$ space group (No. 229) with Tb, Pd, Ga1, and Ga2 occupying the 8*c*, 2*a*, 12*d* and 12*e* sites, respectively. The crystal structure consists of corner-sharing MGa_6 octahedra and $TbGa_3$ cuboctahedra alternating along both the *ab*-plane and the *c*-axis. The bonding distances in the cuboctahedra are listed in Table 3.

The MGa_6 octahedron in Tb_4MGa_{12} (M = Pd, Pt) is isostructural to the $AgCa_6$ octahedron in the Ag_8Ca_3 structure type, a body centered cubic cell [31]. The Pd–Ga interatomic distance in the octahedra in Tb_4PdGa_{12} is 2.540(4) Å, which is shorter than the summation of the covalent radii for Pd (1.37 Å) and Ga (1.22 Å) [32]. The Pt–Ga interatomic distance in the octahedra in Tb_4PtGa_{12} is 2.5341(3) Å, which is within the expected interatomic distance of 2.61 Å from the summation of the covalent radii of Pt (1.32 Å) and Ga (1.22 Å) [32]. The experimental interatomic distances in Tb_4MGa_{12} (M = Pd, Pt) are comparable to M-Ga (M = transition metal) interatomic distances in the M–Ga octahedra of $Ce_8Pd_{24}Ga$ which range from 2.633 to 2.927 Å [33,34]. The Pd–Ga distance is 2.5609(4), 2.635(7), and 2.623(5) Å in $CePdGa_6$, TbPdGa, and ErPdGa, respectively [11,22]. Similar to $RE_4FeGa_{12-x}Ge_x$ [26] and R_4MGa_{12} (R = Gd–Lu; M = Ni, Pd) [27], the transition metal in Tb_4MGa_{12}

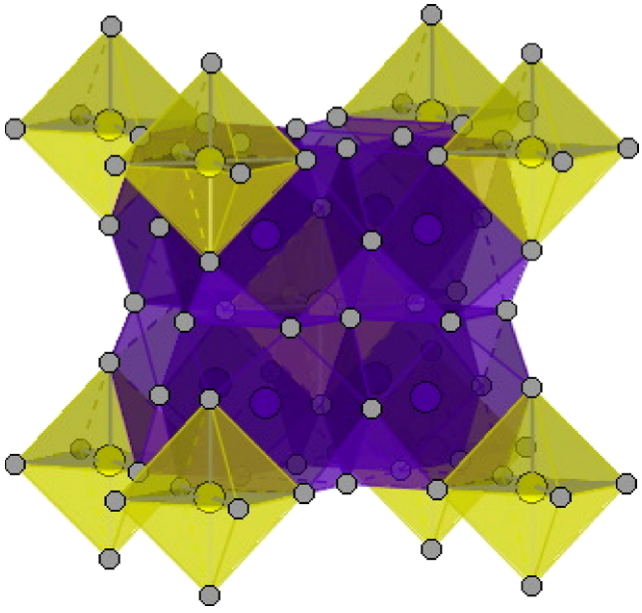

Fig. 1. The crystal structure of Tb_4PdGa_{12} is shown above. $TbGa_3$ cuboctahedra are shown in dark gray and $PdGa_6$ octahedra are shown light gray. Ga atoms are shown as white circles.

(M = Pd, Pt) occupy a unique crystallographic site (2*a*). However, in $RE_4M_7Ge_6$ (M = Ru, Os, Rh, Ir) [35], $M_4Co_7Ge_6$ (M = Zr, Hf) [36], $Np_4Ru_7Ge_6$ [37], $Sc_4M_7Ge_6$ [38] and $U_4Re_7Si_6$ [28] the transition metal occupies two crystallographic sites (2*a* and 12*d*). The transition metal in gallium containing compounds tends to occupy the 2*a* crystallographic site, as is the case in Tb_4MGa_{12}. Indeed, when gallium is present the transition metal occupies the crystallographic site with the lowest multiplicity, while the higher multiplicity site is stabilized with gallium [26].

The Tb cuboctahedra in Tb_4PdGa_{12} is composed of six Tb–Ga(1) distances of 3.03844(18) Å along the *a*-*b* axis and six Tb–Ga(2) distances of 3.0641(4) Å along the *c*-axis. These distances are comparable to the interatomic distances expected from the summation of the atomic radii for Tb (1.75 Å) and Ga (1.26 Å) [32], as well as, the typical interatomic distances in $TbGa_2$ [39] and $TbGa_6$.However, the cuboctahedra found in $LaMIn_5$ are composed of $4 \times$ La–In(1) and $8 \times$ La–In(2) [40]. The La–In2/La–In1 ratio of distances in the cuboctahedra is 1.0110, 1.0000, and 0.99720 for $LaCoIn_5$, $LaRhIn_5$, and $LaIrIn_5$, respectively indicating the Rh compound is the least distorted [40]. The ratio between the Tb–Ga2 and Tb–Ga1 distances in Tb_4PdGa_{12} is 1.000845 and 1.00813 in Tb_4PtGa_{12}, indicating that the cuboctahedra in these phases are highly symmetric.

The Ga–Ga interatomic distance is 2.7730(4) and 2.7746(2) Å for Tb_4PdGa_{12} and Tb_4PtGa_{12}, respectively. Both of these are longer than the interatomic distances expected by the summation of the covalent radii previously mentioned, but they are well within the range of 2.297(5)–2.830(7) Å distances reported in $CeGa_6$,[41] $CeGa_2$,[42] and $CePdGa_6$ [11].

3.2. Physical properties

Fig. 2 shows the temperature dependence of the susceptibility for Tb_4PdGa_{12} taken in a constant field of 1000 G. The antiferromagnetic transition with a Néel temperature at $T_N = 16$ K is very sharp, and a second transition is observed near 2.1 K. Above T_N the susceptibility obeys the Curie–Weiss law, and the linear behavior expected in $1/\chi$ vs. T is shown in the inset of Fig. 2. Fitting the data to the following form: $\chi(T) = C/(T-\theta)$, we find an effective magnetic moment of 7.6 μ_B per Tb ion and a Weiss temperature $\theta = -31.5$ K, indicating strong antiferromagnetic correlations. The effective moment is somewhat smaller than that expected for Tb^{3+} (9.7 μ_B) but is close to the value for Tb^{4+} (7.9 μ_B).

Fig. 3 shows the temperature dependence of the magnetic susceptibility for Tb_4PtGa_{12}. A sharp antiferromagnetic transition takes place at $T_N = 12$ K, and, as in the Pd compound, a smaller transition appears near 2 K From the Curie–Weiss fit (inset Fig. 3) we

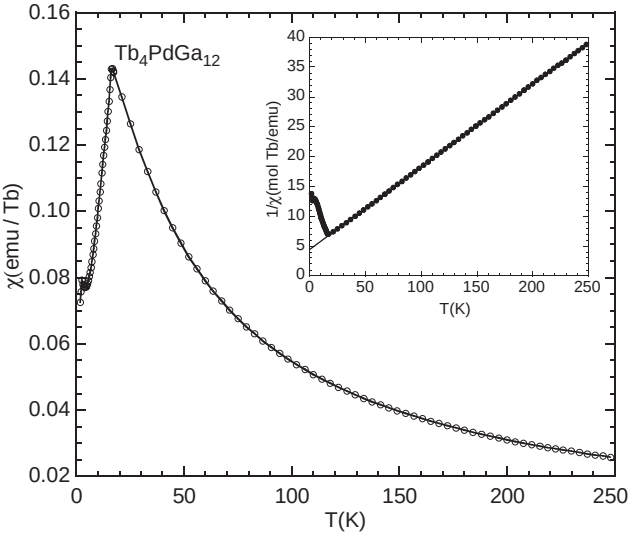

Fig. 2. The susceptibility of Tb_4PdGa_{12} as a function of T measured at 1000 G. The inset figure shows the inverse susceptibility versus temperature of Tb_4PdGa_{12}.

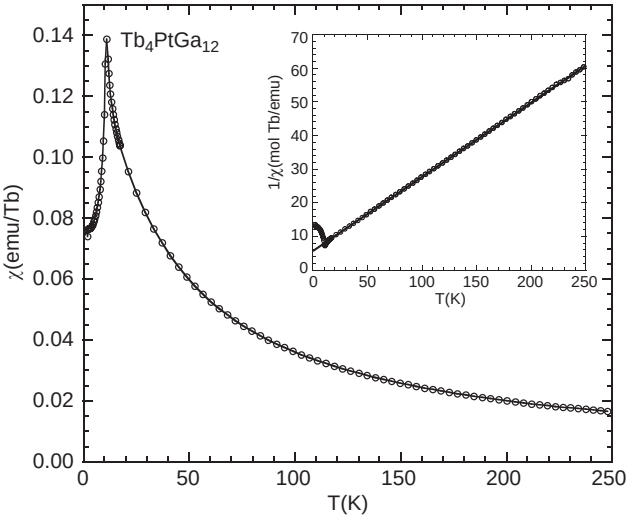

Fig. 3. The susceptibility of Tb_4PtGa_{12} as a function of T, measured at 1000 G. The inset figure shows the inverse susceptibility versus temperature of Tb_4PtGa_{12}.

obtain an effective magnetic moment of 6.2 μ_B per Tb ion and a Weiss temperature $\theta = -25.8$ K. In this case, the effective moment is smaller than what is expected for either Tb^{3+} or Tb^{4+}. Therefore, the Tb valence in Tb_4PtGa_{12} cannot be deduced from the susceptibility measurements. Experimentally measuring an effective moment below the full Hund's rule value is not uncommon in Tb compounds [20,21]. Neutron diffraction and specific heat measurements in magnetic field will be useful in determining the magnetic structure of these two compounds and are planned for the near future.

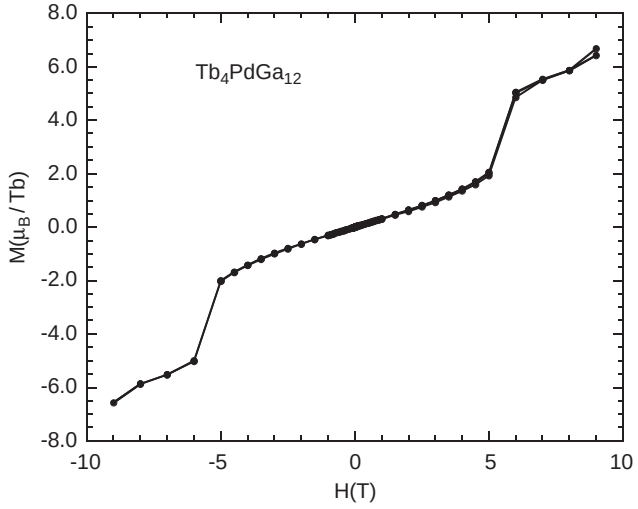

Fig. 4. The magnetization M of Tb_4PdGa_{12} as a function of field, measured at 2 K.

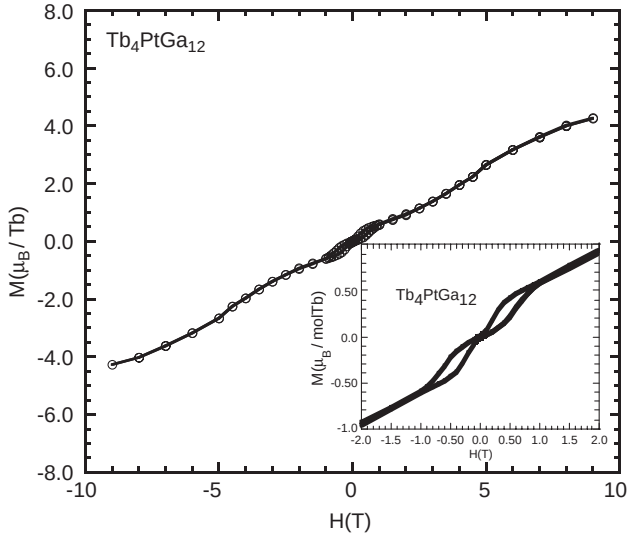

Fig. 5. The magnetization M of Tb_4PtGa_{12} as a function of field, measured at 2 K.

The field-dependent magnetization at 2 K for Tb_4PdGa_{12} is shown in Fig. 4. The magnetization has not saturated at 9 T, and a non-hysteretic metamagnetic transition is observed at ± 5 T. For Tb_4PtGa_{12} the field-dependent magnetization is shown in Fig. 5. Again, the magnetization is not saturated at 9 T and metamagnetic transitions can be seen at ± 0.3 T. This transition is hysteretic in field (inset Fig. 5). Similar hysteresis loops have been observed in other Tb compounds, such as $TbGa_2$ [24].

The electrical resistivity of single crystals of Tb_4PdGa_{12} and Tb_4PtGa_{12} is shown as a function of temperature in Fig. 6. The samples are metallic ($d\rho/dT > 0$), with residual resistance ratios (RRR) of 4 and 7 for Tb_4PtGa_{12} and Tb_4PdGa_{12}, respectively. A

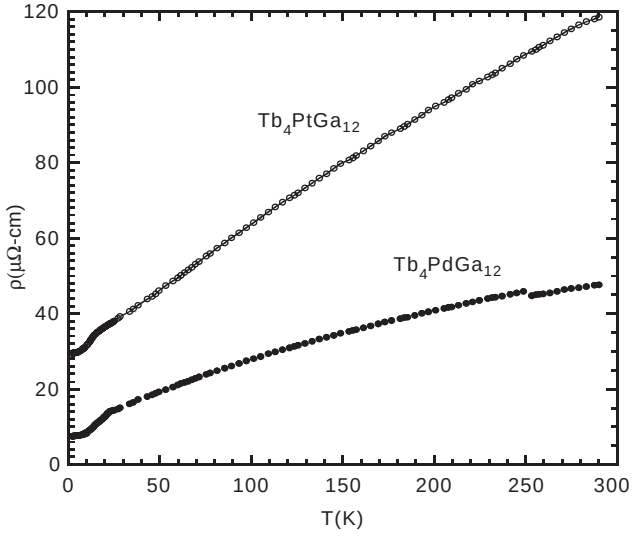

Fig. 6. The electrical resistivity of Tb_4PdGa_{12} (solid circle) and Tb_4PtGa_{12} (open circle) as a function of temperature.

kink in the resistivity is observed for each compound near its antiferromagnetic ordering temperature, indicating a decrease in the spin-disorder scattering.

The structure and preliminary magnetization studies warrant further investigation. It would be of interest to grow the high temperature polymorph of $TbGa_3$ [43], which is isostructural to the antiferromagnetic heavy fermion $CeIn_3$. Compounds of the R_4MGa_{12} structure type can provide the opportunity to compare the influence of the rare earth atom in the cuboctahedra coordination. High pressure and ambient pressure heat capacity experiments are in progress.

Acknowledgments

J.Y.C. acknowledges the NSF Career (DMR 0237664) and Alfred P. Sloan Fellowship for partial support of this project.

References

[1] H. Hegger, C. Petrovic, E.G. Moshopoulou, M.F. Hundley, J.L. Sarrao, Z. Fisk, J.D. Thompson, Phys. Rev. Lett. 84 (2000) 4986.
[2] C. Petrovic, P.G. Pagliuso, M.F. Hundley, R. Movshovich, J.L. Sarrao, J.D. Thompson, Z. Fisk, P. Monthoux, J. Phys. Condens. Matter 13 (2001) L337.
[3] C. Petrovic, R. Movshovich, M. Jaime, P.G. Pagliuso, M.F. Hundley, J.L. Sarrao, Z. Fisk, J.D. Thompson, Europhys. Lett. 53 (2001) 354.
[4] J.D. Thompson, R. Movshovich, Z. Fisk, F. Bouquet, N.J. Curro, R.A. Fisher, P.C. Hammel, H. Hegger, M.F. Hundley, M. Jaime, P.G. Pagliuso, C. Petrovic, N.E. Phillips, J.L. Sarrao, J. Magn. Mater. 226 (2001) 5.
[5] Y.N. Grin, Y.P. Yarmolyuk, E.I. Gradyshevsky, Kristallografiya 24 (1979) 242.
[6] E.G. Moshopoulou, Z. Fisk, J.L. Sarrao, J.D. Thompson, J. Solid State Chem. 158 (2001) 25.

[7] E.G. Moshopoulou, J.L. Sarrao, P.G. Pagliuso, N.O. Moreno, J.D. Thompson, Z. Fisk, R.M. Ibberson, Appl. Phys. A—Mater. Sci. Process. 74 (2002) S895.
[8] W. Bao, P.G. Pagliuso, J.L. Sarrao, J.D. Thompson, Z. Fisk, J.W. Lynn, Phys. Rev. B 6402 (2001).
[9] R.T. Macaluso, J.L. Sarrao, N.O. Moreno, P.G. Pagliuso, J.D. Thompson, F.R. Fronczek, M.F. Hundley, A. Malinowski, J.Y. Chan, Chem. Mater. 15 (2003) 1394.
[10] N.D. Mathur, F.M. Grosche, S.R. Julian, I.R. Walker, D.M. Freye, R.K.W. Haselwimmer, G.G. Lonzarich, Nature 394 (1998) 39.
[11] R.T. Macaluso, S. Nakatsuji, H. Lee, Z. Fisk, M. Moldovan, D.P. Young, J.Y. Chan, J. Solid State Chem. 174 (2003) 296.
[12] J.N. Millican, R.T. Macaluso, D.P. Young, M. Moldovan, J.Y. Chan, J. Solid State Chem., 2004, in press.
[13] D.T. Adroja, W. Kockelmann, A.D. Hillier, J.Y. So, K.S. Knight, B.D. Rainford, Phys. Rev. B 67 (2003).
[14] S. Chastin, D.T. Adroja, D.F. Brewer, T. Hargreaves, C.S. McMenamin, B.D. Rainford, A.L. Thomson, Czech. J. Phys. 46 (1996) 2589.
[15] T. Burghardt, E. Hallmann, A. Eichler, Physica B 230 (1997) 214.
[16] E. Bauer, R. Hauser, E. Gratz, G. Schaudy, M. Rotter, A. Lindbaum, D. Gignoux, D. Schmitt, Z. Phys. B—Condens. Matter 92 (1993) 411.
[17] K. Terayama, Y. Aoki, H. Sato, J. Phys. Condens. Matter 7 (1995) 6899.
[18] W.M. Williams, R.T. Macaluso, M. Moldovan, D.P. Young, J.Y. Chan, Inorg. Chem. 42 (2003) 7315.
[19] J.K. Yakinthos, P.A. Kotsanidis, W. Schafer, G. Will, J. Magn. Magn. Mater. 81 (1989) 163.
[20] P. Schobinger-Papamantellos, F. Fauth, D.P. Middleton, K.H.J. Buschow, J. Alloy. Compd. 252 (1997) 16.
[21] C.D. Routsi, J. Alloy Compd. 319 (2001) 85.
[22] B. Penc, M. Hofmann, J. Leciejewicz, A. Szytula, A. Zygmunt, J. Alloy Compd. 305 (2000) 24.
[23] B. Penc, A. Szytula, J. Hernandez-Velasco, A. Zygmunt, J. Magn. Magn. Mater. 256 (2003) 373.
[24] H. Asmat, D. Gignoux, R. Lemaire, Physica B & C 86 (1977) 185.
[25] E. Lidstrom, R. Wappling, O. Hartmann, M. Ekstrom, G.M. Kalvius, J. Phys.Condens. Matter 8 (1996) 6281.
[26] M.A. Zhuravleva, X.P. Wang, A.J. Schultz, T. Bakas, M.G. Kanatzidis, Inorg. Chem. 41 (2002) 6056.
[27] L.O. Vasilenko, A.S. Noga, Y.N. Grin, M.D. Koterlin, Y.P. Yarmolyuk, Russ. Metall., 1988, p. 216.
[28] L.G. Akselrud, J.P. Jarmoljuk, E.I. Gladyshevskij, Dopov Akad Nauk, 1978, p. 359.
[29] K. Doi, N. Masaki, Acta Crystallogr. A 26 (1970) 443.
[30] G.M. Sheldrick, Program for Refinement of Crystal Structures, vol.54, University of Göttingen, Germany, 1997, p. 443.
[31] G.J. Snyder, A. Simon, Angew. Chem.-Int. Ed. Engl. 33 (1994) 689.
[32] L. Sutton, The Chemical Society: London 'Vol.' Spec. Publ. No. 18, 1965.
[33] R.A. Gordon, F.J. DiSalvo, Z. Naturforsch. B 51 (1996) 52.
[34] R.A. Gordon, F.J. DiSalvo, Physica B 225 (1996) 23.
[35] M. Francois, G. Venturini, J.F. Mareche, B. Malaman, B. Roques, J. Less-Common Met. 113 (1985) 231.
[36] A.I. Zyubrik, R.R. Olenych, Y.P. Yarmolyuk, Dopov. Akad. Nauk Ukr. Rsr Ser. A, 1982. p. 74.
[37] F. Wastin, J. Rebizant, J.P. Sanchez, A. Blaise, J. Goffart, J.C. Spirlet, C.T. Walker, J. Fuger, J. Alloy. Compd. 210 (1994) 83.
[38] N. Engel, B. Chabot, E. Parthe, J. Less-Common Met. 96 (1984) 291.
[39] A. Raman, Z. Metallkd. 58 (1967) 179.
[40] R.T. Macaluso, J.L. Sarrao, P.G. Pagliuso, N.O. Moreno, R.G. Goodrich, D.A. Browne, F.R. Fronczek, J.Y. Chan, J. Solid State Chem. 166 (2002) 245.
[41] G. Kimmel, D. Dayan, A. Grill, J. Pelleg, J. Less-Common Met. 75 (1980) 133.
[42] K. Schubert, H.L. Lucas, H.G. Meibner, S. Bhan, Z. Metallk. 50 (1959) 534.
[43] S. Cirafici, E. Franceschi, J. Less-Common Met. 77 (1981) 269.